Thermochemical solar hydrogen generation

Stuart Licht*

Received (in Cambridge, UK) 16th June 2005, Accepted 10th August 2005
First published as an Advance Article on the web 30th August 2005
DOI: 10.1039/b508466k

Solar direct, indirect and hybrid thermochemical processes are presented for the generation of hydrogen and compared to alternate solar hydrogen processes. A hybrid solar thermal/electrochemical process combines efficient photovoltaics and concentrated excess sub-bandgap heat into highly efficient elevated temperature solar electrolysis of water and generation of H_2 fuel utilizing the thermodynamic temperature induced decrease of E_{H_2O} with increasing temperature. Theory and experiment is presented for this process using semiconductor bandgap restrictions and combining photodriven charge transfer, with excess sub-bandgap insolation to lower the water potential, and their combination into highly efficient solar generation of H_2 is attainable. Fundamental water thermodynamics and solar photosensitizer constraints determine solar energy to hydrogen fuel conversion efficiencies in the 50% range over a wide range of insolation, temperature, pressure and photosensitizer bandgap conditions.

Department of Chemistry, University of Massachusetts Boston, Boston, MA 02125-3393, USA. E-mail: stuart.licht@umb.edu; Fax: 617-287-6030; Tel: 617-287-6130

Stuart Licht is Chair of the Chemistry Department at the University of Massachusetts, Boston, and is the upcoming (2006) recipient of the Electrochemical Society Energy Technology Award for his pioneering contributions in solar energy research. His interests include solar and hydrogen energy, energy storage, unusual analytical methodologies, and fundamental physical chemistry. Professor Licht received his doctorate in 1986 from the Weizmann Institute of Science, followed by appointments as a Postdoctoral Fellow and Visiting Scientist at MIT. In 1988 he was the first Carlson Professor of Chemistry at Clark University, and in 1995 was awarded a Gustella Professorship at the Technion Israel Institute of Science. He has contributed 250 peer reviewed papers and patents ranging from novel efficient solar semiconductor/electrochemical processes, to unusual batteries, to elucidation of complex equilibria and quantum electron correlation theory. He has established the field of Fe(VI) charge storage (Science, 1999; Chem. Comm. 2004), as well as furthering the understanding of batteries (Science, 1993), microelectrodes (Science, 1989), and photoelectrochemical (Nature, 1987, 1990, 1991; Appl. Phys. Lett., 1999; Solar Energy Mat 1994, 1995, 1998, 2002; Chem. Comm. 2003, 2005) energy conversion processes.

Introduction to solar thermal formation of H_2

Comparison of solar hydrogen processes

Solar energy-driven water-splitting combines several attractive features for energy utilization. The energy source (sun) and reactive media (water) for solar water-splitting are readily available and are renewable, and the resultant fuel (generated H_2) and its discharge product (water) are each environmentally benign. Energy conversion, storage and utilization *via* the clean solar water-splitting/hydrogen fuel cycle is summarized in Scheme 1, without (left side) and with (right side) the inclusion of solar energy. This review presents one of the more promising renewable energy sources under consideration, the hybrid thermochemical solar generation of hydrogen. This energy source is capable of sustaining the highest solar energy conversion efficiencies and fits well into a clean hydrogen energy cycle.

To better understand the significance of an efficient solar hydrogen formation process, it is useful to introduce it in the context of other hydrogen technologies. Actualization of a hydrogen, rather than fossil fuel, economy requires H_2 storage, utilization and generation processes; the latter is the least developed of these technologies. H_2 generated from the reforming of fossil fuels would again release carbon dioxide as a greenhouse gas. Solar water-splitting can provide clean, renewable sources of hydrogen fuel without greenhouse gas evolution. A variety of approaches have been studied to achieve this important goal. These include photosynthetic, biological and photochemical solar water-splitting; each has exhibited solar energy-to-hydrogen conversion efficiencies, η_{solar}, of the order of only 1%. Photothermal processes have been reported in the η_{solar} = 1–10% range, and photovoltaic or photoelectrochemical solar water-splitting has reached η_{solar} = 18%.[1–4] The highest solar efficiencies have been observed recently with a hybrid process, which unlike the other

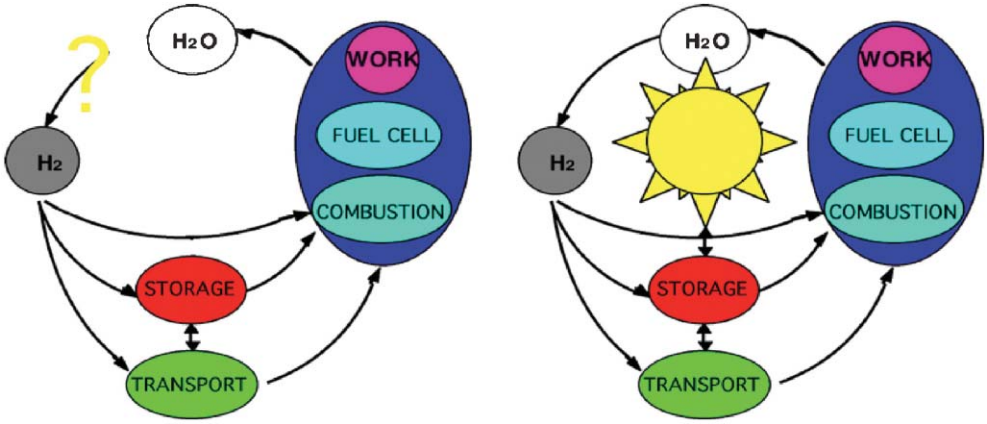

Scheme 1 The hydrogen fuel cycle is an environmentally benign process for the utilization, storage/transport and generation of energy. What will be the energy source to provide H_2 for a hydrogen economy (left)? The right side of the scheme utilizes solar energy in the generation and/or storage of hydrogen fuel.

processes, incorporates full utilization of the solar spectrum, further enhancing achievable solar conversion efficiencies. This hybrid process, combines solar photo- and solar thermal-energy conversion, with high temperature electrochemical water-electrolysis for generation of hydrogen fuel.

Solar thermal, hybrid and photoelectrochemical hydrogen

At high temperatures ($T > 2000$ °C), water chemically disproportionates to H_2 and O_2 (without electrolysis). Hence, in principal, using solar energy to directly heat water to these temperatures, hydrogen can be spontaneously generated. This is the basis for all direct thermochemical solar water-splitting processes.[1] However, catalysis, gas recombination and containment material limitations above 2000 °C have led to very low solar efficiencies for direct solar thermal hydrogen generation. Other thermal approaches are either indirect[2,4] or hybrid processes.[3] Multi-step, indirect, solar thermal reaction processes to generate hydrogen at lower temperatures have been studied, and a variety of pertinent, reaction processes considered. These reactions are conducted in a cycle to regenerate and reuse the original reactions (ideally, with the only net reactant water, and the only net products hydrogen and oxygen). Such cycles suffer from challenges often encountered in multi-step reactions.[2,4] While these cycles can operate at lower temperatures than the direct thermal chemical generation of hydrogen, efficiency losses can occur at each of the steps in the multiple step sequence, resulting in low overall solar-to-hydrogen energy conversion efficiencies.

Electrochemical water-splitting, generating H_2 and O_2 at separate electrodes, largely circumvents the gas recombination and high temperature limitations occurring in thermal hydrogen processes. There has been ongoing experimental and theoretical interest in utilizing solar-generated electrical charge to drive electrochemical water-splitting (electrolysis) for hydrogen generation.[5–10] Early photoelectrochemical models had underestimated low solar water-splitting conversion efficiencies, predicting that a maximum of ~15% would be attainable. This was increased to ~30% solar water-splitting modeled conversion efficiency by eliminating (i) the linkage of photo- to electrolysis-surface area, (ii) non-ideal matching of photo- and electrolysis-potentials, and incorporating the effectiveness of contemporary (iii) electrolysis catalysts and (iv) efficient multiple bandgap photosensitizers.[9] Our experimental water-splitting cell incorporating these features achieved over 18% solar energy-to-hydrogen conversion efficiency, Scheme 2. However, these models and experiments did not incorporate solar heat effects improvements on the electrolysis energetics of charge utilization, or semiconductor imposed heat utilization limitations.

The UV and visible energy-rich portion of the solar spectrum is transmitted through H_2O. Therefore sensitization, such as *via* semiconductors, is required to drive the electrical charge for the water-splitting process. In photoelectrochemical processes, illuminated semiconductors drive redox processes in solution.[11] The principal advantages of photoelectrochemical-(PEC) compared to solid state photovoltaic- (PV) charge transfer, are the possiblity for internal electrochemical charge storage[12–14] and the fact that solution-phase processes can be used to influence the energetics of photo-driven charge transfer.[9,15–18] The principal disadvantage is that exposure to the electrolyte can lead to semiconductor deterioration. PV water-splitting processes utilize a photo-absorber connected *ex situ* by an electronic conductor into the electrolyte, to electrochemically drive water-splitting, *e.g.* an illuminated solar cell wired to an electrolyzer. While PEC water-splitting processes utilize *in situ* immersion of a photo-absorber in a chemical solution, such as an illuminated semiconductor in water for electrochemically driven water-splitting.[19] The significant fundamental components of PV and PEC hydrogen generation are identical, but from a pragmatic viewpoint the PV process seems preferred, as it isolates the semiconductor from contact and corrosion with the electrolyte. Illuminated semiconductors, such as TiO_2 and InP can split water, but their wide bandgap, E_g, limits the photo-response to a small fraction of the incident solar energy, and studies have generally focused on diminishing the high E_g for solar water-splitting, by tuning (decreasing) the E_g of the photosensitizers to better match the water-splitting potential, E_{H_2O}.[20,21] Multiples of electrolyzers and photovoltaics can be combined to produce an efficient

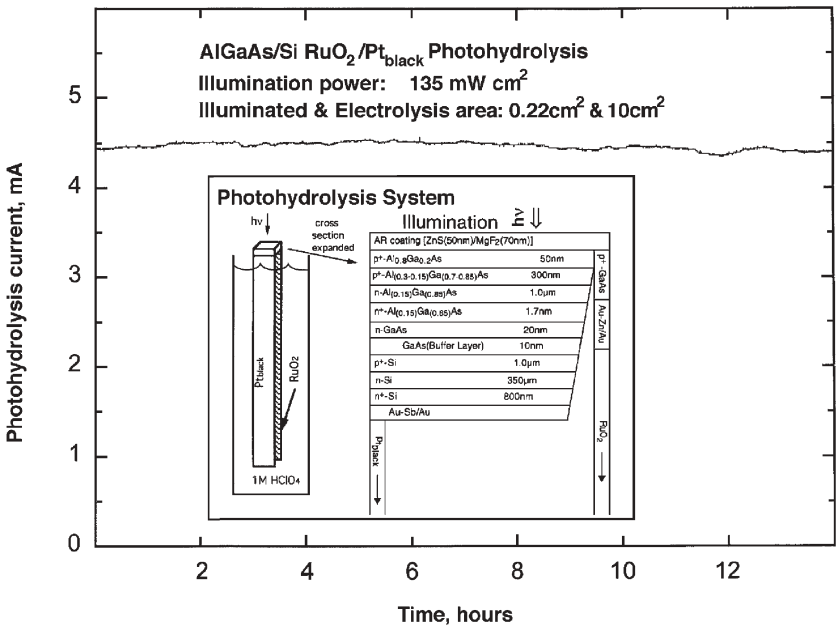

Scheme 2 Representation (inset) and measured characteristics of the illuminated AlGaAs/Si RuO_2/Pt_{black} η_{solar} = 18% photoelectrolysis cell.[9]

match of the generated and consumed power. Also, multiple bandgap semiconductors can be combined to generate a single photovoltage well matched to the electrolysis cell, and over 18% conversion energy efficiency of solar to hydrogen has been demonstrated (Scheme 2) albeit at room temperature (without the benefit of higher efficiency solar thermal processes).[19,22,23]

At higher temperature a hybrid process overcomes the limitations and combines the advantages of photothermal and PV or PEC water splitting processes. IR radiation, is energetically insufficient to drive conventional solar cells. Hence PV and PEC solar electrolysis discard (by reflectance or as re-radiated heat) solar thermal radiation. However, the hybrid process can utilize the full solar spectrum energy leading to substantially higher solar energy efficiencies. As seen in Scheme 3, and as described in a later section of this chapter, in the hybrid process the solar IR is not discarded, but instead separated and utilized to heat water, which substantially decreases the necessary electrochemical potential to split the water and substantially increases the solar hydrogen energy conversion efficiencies.

Direct solar thermal hydrogen generation

Direct thermochemical water splitting consists of heating water to a high temperature and separating the spontaneously formed hydrogen from the equilibrium mixture. Although conceptually simple, this process has been impeded by high

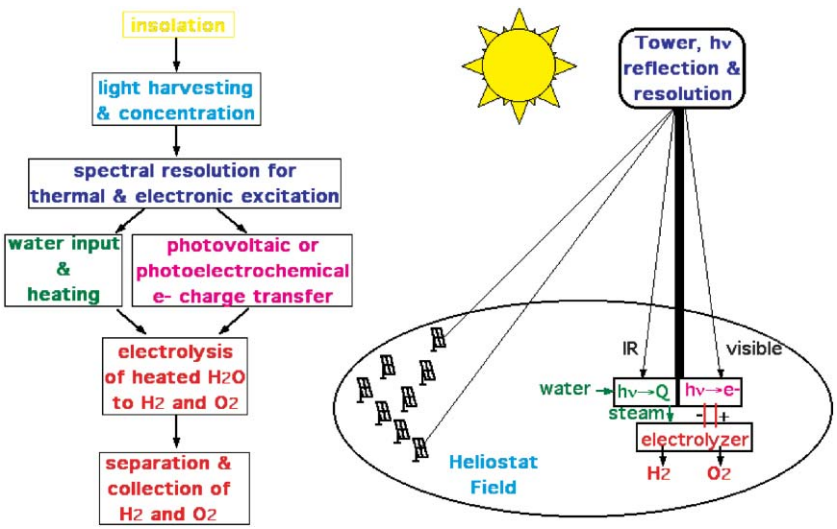

Scheme 3 Solar water electrolysis improvement through excess solar heat utilization *via* thermal electrochemical hybrid H_2 generation.[3]

temperature material limitations and the need to separate H_2 and O_2 to avoid ending up with an explosive mixture. Unfortunately, for thermal water splitting $T > 2500$ K is necessary to achieve a significant degree of hydrogen dissociation. The free energy, ΔG, of the gas reaction $H_2O \leftrightarrows H_2 + \frac{1}{2}O_2$, does not become zero until the temperature is increased to 4310 K at 1 bar pressure of H_2O, H_2 and O_2. Smaller amounts of product are barely discernable at 2000 K.[3] The entropy, ΔS, driving the negative of the temperature derivative of the free energy of water, is simply too small to make direct decomposition feasible at this time.[4]

The production of hydrogen by direct thermal splitting of water generated a considerable amount of research during the period 1975–1985. Fletcher and co-workers in the USA stressed the thermodynamic advantages of a one-step process with heat input at as high a temperature as possible.[25] The theoretical and practical aspects were examined by Lede and others.[1,26] The main emphases in these investigations were the thermodynamics and the demonstration of the feasibility of the process. However, no adequate solution to the crucial problem of separation of the products of water-splitting has been worked out so far, although effort was devoted to demonstrate the possibility of product separation at low temperature, after quenching the hot gas mixtures by heat exchange cooling, by immersion of the irradiated, heated target in a reactor of liquid water, by rapid turbulent gas jets, or rapid quenching by injection of a cold gas.[2]

In order to attain efficient collection of solar radiation in a solar reactor operating at the requisite 2500 K, it is necessary to reach a high radiation concentration of the order 10 000. For example a 3 MW solar tower facility consists of a field of 64 50× concentrating heliostats. By directing all the heliostats to reflect the sun's rays towards a common target, a concentration ratio of only 3000 may be obtained, and to enhance this requires a secondary concentration optical system.[27]

Ordinary steels can't resist temperatures above a few hundred degrees centigrade, while the various stainless steels, including the more exotic ones, fail at less than 1300 K. In the range 3000–1800 C alumina, mullite or fused silica may be used. A temperature range of about 2500 K requires the use of special materials for the solar reactor. Higher melting point materials can have additional challenges; carbide or nitride composites are likely to react with water splitting products at the high temperatures needed for the reaction.[1]

When the high temperature gas phase equilibrium of water occurs, in addition to H_2O, H_2 and O_2, the atomic components H and O need to be considered. The fraction of these species is relatively insignificant at temperatures below 2500 K, as the pressure equilibrium constants for either diatomic hydrogen or oxygen formation from their atoms are each greater than 10^3 at $T \leqslant 2500$ K. However, the atomic components become increasingly significant at higher temperatures. The pressure equilibrium constants of the water dissociation reaction over a range of temperatures[24] are summarized in eqn. (1) for the relevant four equilibria, and their associated equlibrium constants K_i, considered for the water-splitting at temperatures in which significant, spontaneous formation of H_2 occurs:

$$\begin{gathered} H_2O \leftrightarrows HO + H\ (K_1) \\ HO \leftrightarrows H + O\ (K_2) \\ 2H \leftrightarrows H_2\ (K_3) \\ 2O \leftrightarrows O_2\ (K_4) \end{gathered} \tag{1}$$

	$T = 2500$ K	$T = 3000$ K	$T = 3500$ K
K_1	1.34×10^{-4}	8.56×10^{-3}	1.68×10^{-1}
K_2	4.22×10^{-4}	1.57×10^{-2}	2.10×10^{-1}
K_3	1.52×10^{3}	3.79×10^{1}	2.67×10^{0}
K_4	4.72×10^{3}	7.68×10^{1}	4.01×10^{0}

Kogan has calculated that at a pressure of 0.05 bar water dissociation is barely discernible at 2000 K. By increasing the temperature to 2500 K, 25% of water vapor dissociates at the same pressure. A further increase in temperature to 2800 K under constant pressure causes 55% of the vapor to dissociate.[1] These basic facts reflect the challenges that must be overcome for practical hydrogen production by a solar thermal water-splitting process: (a) attainment of very high solar reactor temperatures, (b) solution of the materials problems connected with the construction of a reactor that can contain the water-spitting products at the reaction temperature and (c) development of an effective method of *in situ* separation of hydrogen from the mixture of water-splitting.

Separation of the generated hydrogen from the mixture of the water-splitting products, to prevent explosive recombination, is another challenge for thermochemically generated water-splitting processes. From the perspective of the high molecular weight ratio of oxygen and hydrogen, separation of the thermochemically generated hydrogen from the mixture of the water-splitting products by gas diffusion through a porous ceramic membrane can be relatively effective. Membranes that have been considered include commercial and specially prepared porous zironcias, although sintering was observed to occur under thermal water-splitting conditions,[1,28] and ZrO_2–TiO_2–Y_2O_3 oxides.[29] In such membranes, it is necessary to maintain a Knudsen Flow regime across the porous wall.[24] The molecular mean free path λ in the gas must be greater than the average pore diameter ϕ.[1] A double-membrane configuration has been suggested as superior to a single-membrane reactor.[30]

In recent times, there have been relatively few studies on the direct thermochemical generation of hydrogen by water-splitting[1,24,28–31] due to continuing high temperature material limitations. Principal recent experimental work has been performed by Kogan and associates.[1,28] In 2004, Bayara reiterated that conversion rates in direct thermochemical processes are still quite low and new reactor designs, operation schemes and materials are needed for a new breakthrough in this field.[31]

Indirect (multistep) solar thermal H_2 generation

Indirect solar thermal splitting of water utilizes a reaction sequence, whose individual steps require lower temperatures than the direct solar thermal process. Historically, the reaction of reactive metals and reactive metal hydrides with water or

acid was the standard way of producing pure hydrogen. These reactions involved sodium metal or calcium hydride with water, or zinc metal with hydrochloric acid, or metallic iron or ferrous oxide with steam, to produce H_2. All these methods are quite outdated and expensive.

Multi-reaction processes to produce hydrogen from water, with a higher thermal efficiency have been extensively studied. As summarized in Fig. 1 a variety of pertinent, spontaneous processes can be considered which have a negative reaction free energy at temperatures considerably below that for water. These reactions are conducted in a cycle to regenerate and reuse the original reactions (ideally, with the only net reactant water and the only net products hydrogen and oxygen). While these cycles operate at much lower temperatures than the direct thermal chemical generation of hydrogen, conversion efficiencies are insufficient and interest in these cycles has waned. Efficiency losses can occur at each of the steps in the multiple step sequence, resulting in low overall solar-to-hydrogen energy conversion efficiencies. Interest in indirect thermal chemical generation of hydrogen started approximately 40 years ago. An upsurge in interest occurred with an average of over 70 papers per year from 1975 through 1985. Following that time, and the lack of clear success, publications have diminished to approximately 10 per year.[4] An overview of indirect thermochemical processes for hydrogen generation has been presented by Funk, with 2 to 6 steps in the total reaction cycle, each operating at a maximum temperature of 920 to 1120 K.[4]

Status reviews on multiple-step cycles have been presented[2,4,32] and leading candidates include a 3-step cycle based on the thermal decomposition of H_2SO_4 at 1130 K, and a 4-step cycle based on the hydrolysis of $CaBr_2$ and $FeBr_2$ at 1020 and 870 K: This process involving two Ca and two Fe compounds at $T \leqslant 1050$ K has received some attention.[4] The process is operated in a cyclic manner in which the solids remain in their reaction vessels and the flow of gases is switched when the desired reaction extent is reached. This can be summarized as follows:

$$\begin{gathered} CaBr_2(s) + H_2O(l) \rightarrow CaO(s) + 2HBr(g) \\ CaO(s) + Br_2(g) \rightarrow CaBr_2(s) + O_2(g) \\ Fe_3O_4(s) + 8HBr(g) \rightarrow 3FeBr_2(s) + 4H_2O(g) + 2Br_2(g) \\ 3FeBr_2(s) + 4H_2O(g) \rightarrow Fe_3O_4(s) + 6HBr(g) + H_2(g) \end{gathered} \quad (2)$$

One of the most actively studied candidate metal oxide redox pairs for the 2-step cycle reactions is ZnO/Zn. Several chemical aspects of the thermal dissociation of ZnO have been investigated including reaction rates, Zn separation, and heat recovery in the presence of O_2. Cycles incorporating ZnO continue to be of active research interest.[2,33–36]

Higher temperatures, are needed for more efficient indirect solar thermal processes, such as two-step thermal chemical cycles using metal oxide reactions.[2] The first step is solar thermal, the metal oxide endothermic dissociation to a lower-valence, or to the metal. The second step is non-solar, and is the exothermic hydrolysis of the metal to form H_2 and the corresponding metal oxide. The net reaction remains $H_2O = H_2 + \frac{1}{2}O_2$, but as H_2 and O_2 are formed in different steps, the need for high-T gas separation is thereby eliminated.

$$\begin{gathered} \text{1st step (solar): } M_xO_y \rightarrow xM + y/2O_2 \\ \text{2nd step (non-solar): } xM + yH_2 \rightarrow M_xO_y + yH_2 \end{gathered} \quad (3)$$

where M is a metal and M_xO_y is the corresponding metal oxide. The redox pairs Fe_3O_4/FeO, TiO_2/TiO_x, Mn_3O_4/MnO, Co_3O_4/CoO and MnO with NaOH have been studied and also the mixed metal oxides of the type $(Fe_{1-x}M_x)_3O_4/(Fe_{1-x}M_x)_{1-y}O$.[2,33,36] These processes retain many of the $T > 2000$ K material challenges faced by direct thermal water-splitting.

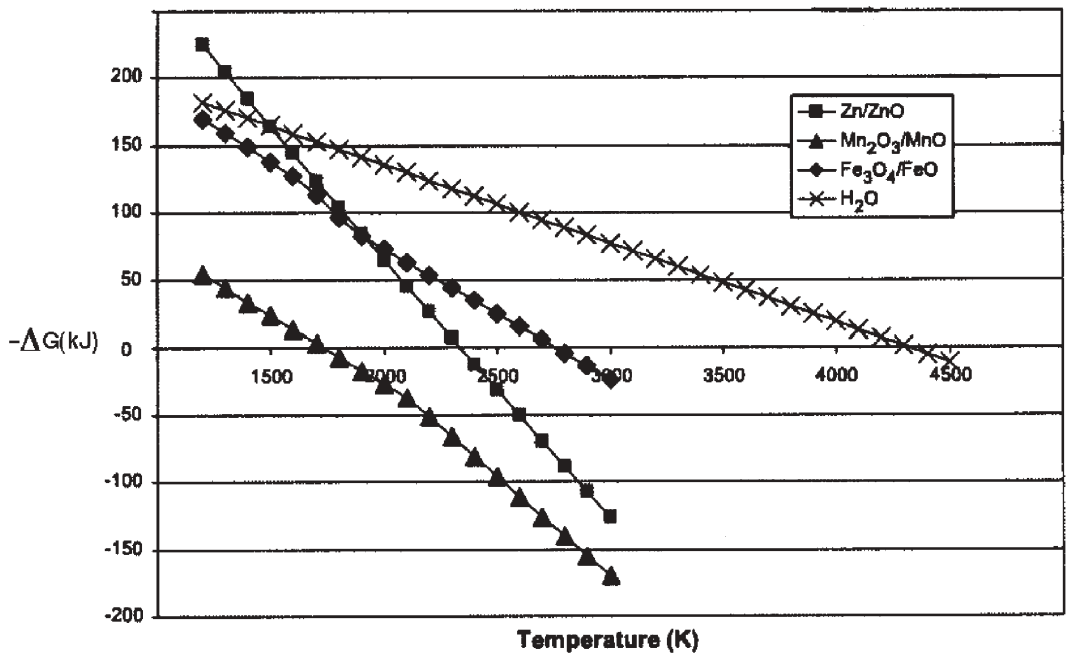

Fig. 1 Temperature variation of the free energy for several decomposition reactions pertinent to hydrogen generation. Modified from ref. 34.

Solar-thermal/electrochemical/photo-hydrogen

Development of hybrid thermal hydrogen generation

Nicholson and Carlisle first generated hydrogen by water electrolysis in 1800. Modifications, such as steam electrolysis, or illuminated semiconductor electrolysis,[20] had been reported by the 1970s. The electrolysis of water, can be substantially enhanced by heating the water with excess solar thermal energy. This hybrid solar hydrogen process is delineated in this section. Fundamental water thermodyanmics and solar photosensitizer constraints will be shown to be consistent with hybrid solar-to-hydrogen fuel conversion efficiencies in the 50% range, over a wide range of insolation, temperature, pressure and photosensitizer bandgap conditions.

With increasing temperature, the quantitative decrease in the electrochemical potential necessary to split water to hydrogen and oxygen had been well known by the 1950's,[36] and as early as 1980 Bockris noted from this relationship, that solar thermal energy could decrease the necessary energy for the electrolytic generation of hydrogen.[37] However, the process combines elements of solid state physics, insolation and electrochemical theory, complicating rigorous theoretical support of the process. Our fundamental thermodynamic feasibility of the solar thermal electrochemical generation of hydrogen was initially derived in 2002.[38,39] The novel theory combines photo-driven charge transfer, with excess sub-bandgap insolation to lower the water potential, and derives rigorous semiconductor bandgap restricted, thermally enhanced, solar water-splitting efficiencies in excess of 50%. In 2004 experimental support, which is described in the latter sections, was provided in support of the theory.[40]

Theory of efficient solar thermal hybrid/H_2 processes

Thermally-assisted solar electrolysis consists of (i) light harvesting, (ii) spectral resolution of thermal (sub-bandgap) and electronic (super-bandgap) radiation, the latter of which (iiia) drives photovoltaic or photoelectrochemical charge transfer $V(iH_2O)$, while the former (iiib) elevates water to temperature T, and pressure, p; finally (iv) $V(iH_2O)$ driven electrolysis of $H_2O(T,p)$. This solar thermal water electrolysis assisted process (photothermal electrochemical water-splitting) is presented in Scheme 3. Rather than a field of concentrators, systems may use individual solar concentrators. This hybrid process provides a pathway for efficient solar energy utilization. Electrochemical water-splitting, generating H_2 and O_2 at separate electrodes, circumvents the gas recombination limitations or multiple-step repeated Carnot losses of solar thermochemical H_2 formation. This section provides a novel hybrid high temperature process with derivation of bandgap-restricted thermally-enhanced solar water-splitting efficiencies. As discussed in the earlier sections, our previous model had described ambient temperature solar/H_2 energy conversion processes, and predicted limits of $\sim$30% solar energy water-splitting conversion efficiency at room temperature. However, this model did not incorporate the potential benefits (and constraints) of available excess heat.

Photo-driven charge transfer through a semiconductor junction does not utilize photons which have energy below the semiconductor bandgap. Hence a silicon photovoltaic device does not utilize radiation below its bandgap of $\sim$1.1 eV, while a AlGaAs/GaAs multiple bandgap photovoltaic does not utilize radiation of energy less than the 1.43 eV bandgap of GaAs. This unutilized, available long wavelength insolation represents a significant fraction of the solar spectrum, and can be separated to heat water prior to electrolysis. The thermodynamics of heated water dissociation are more favorable than at room temperature. This is expressed by a decrease in the requisite water electrolysis potential, which can considerably enhance solar water-splitting efficiencies.

The H_2-generating water-splitting reaction spontaneity is determined by water's free energy of formation, ΔG°_f, which *via* the Faraday constant, F, yields the water electrolysis rest potential, $E^\circ_{H_2O}$:

$$\begin{gathered} H_2O \rightarrow H_2 + \tfrac{1}{2}O_2 \\ -\Delta G^\circ_{split} = \Delta G^\circ_f\,(25\ ^\circ C, 1\ bar, H_2O_{liq}) = -237.1\ kJ\ mol^{-1} \\ E^\circ_{H_2O}(25\ ^\circ C,\ 1\ bar,\ H_2O_{liq}) = \Delta G^\circ_f(H_2O)/2F = 1.229\ V \end{gathered} \quad (4)$$

Reaction 4 is endothermic, and electrolyzed water will cool unless external heat is supplied. The enthalpy balance and its related thermoneutral potential, E_{tneut}, are given by:

$$\begin{gathered} -\Delta H^\circ_{split} = \Delta H^\circ_f\,(25\ ^\circ C, 1\ bar, H_2O_{liq}) = -285.8\ kJ\ mol^{-1} \\ E_{tneut}{}^\circ(25\ ^\circ C, 1\ bar, H_2O_{liq}) = -\Delta H_f(H_2O_{liq})/2F = 1.481\ V \end{gathered} \quad (5)$$

The water electrolysis rest potential, eqn. (4), is determined from extrapolation to ideal conditions. Variations of the concentration, c, and pressure, p, from ideality are respectively expressed by the activity (or fugacity for a gas), as $a = \gamma c$ (or γp for a gas), with the ideal state defined at 1 atmosphere for a pure liquid (or solid), and extrapolated from $p = 0$ or for a gas or infinite dilution for a dissolved species. The formal potential, measured under real conditions of c and p can deviate significantly from the (ideal thermodynamic) rest potential, as for example the activity of water, a_w, at, or near, ambient conditions generally ranges from approximately 1 for dilute solutions to less than 0.1 for concentrated alkaline and acidic electrolytes.[41–43] The potential for the dissociation of water decreases from 1.229 V at 25 °C in the liquid phase to 1.167 V at 100 °C in the gas phase. Above the boiling point, pressure is used to express the variation of water activity. The variations of the electrochemical potential for water in liquid and gas phases are given by:

$$\begin{gathered} \text{For } A = (\gamma_{H_2} p_{H_2} \gamma_{O_2} p_{O_2})^{1/2} \\ E(H_2O_{liq}) = E^\circ(H_2O_{liq}) + (RT/2F)\ln(A/a_w) \\ E(H_2O_{gas}) = E^\circ(H_2O_{gas}) + (RT/2F)\ln(A/\gamma_{H_2O} p_{H_2O}) \end{gathered} \quad (6)$$

The critical point of water is 374 °C and 221 bar. Below the boiling point, $E^\circ_{H_2O}$ is similar for 1 bar and high water pressure, but diverges sharply above these conditions. Values of $E^\circ_{H_2O}$(1 bar) at 25, 100, 1000 and 1500 °C respectively are 1.229 V, 1.167 V, 0.919 V and 0.771 V; and $E^\circ_{H_2O}$(500 bar) at 100 and 1000 °C are 1.163 V and 0.580 V, respectively. Due to overpotential losses, ζ, the necessary applied potential to drive water electrolyis, V_{H_2O}, is:

$$V_{H_2O}(T) = E^\circ_{H_2O}(T) + \zeta_{anod} + \zeta_{cathod} = (1 + \zeta)\, E^\circ_{H_2O}(T) \quad (7)$$

The water electrolysis potential energy conversion efficiency occurring at temperature, T, is $\eta_{echem}(T) \equiv E^{\circ}_{H_2O}(T)/V_{H_2O}(T)$. Solar water-splitting processes utilize ambient temperature water as a reactant. An interesting case occurs if heat is introduced into the system; that is when electrolysis occurs at an elevated temperature, T, using water heated from 25 °C. The ratio of the standard potential of water at 25° and T, is $r = E^{\circ}_{H_2O}(25\ ^{\circ}C)/E^{\circ}_{H_2O}(T)$. As shown in Fig. 2 $E^{\circ}_{H_2O}(T)$ diminishes with increasing temperature. Hence, an effective water-splitting energy conversion efficiency of $\eta'_{echem} > 1$ can occur, to convert 25 °C water to H_2 by electrolysis at T:

$$\eta'_{echem} = r\eta_{echem}(T) = E^{\circ}_{H_2O}(25\ ^{\circ}C)/V_{H_2O}(T) \qquad (8)$$

For low overpotential electrolysis, $V_{H_2O}(T > 25\ ^{\circ}C)$ can be less than $E^{\circ}_{H_2O}(25\ ^{\circ}C)$, resulting in $\eta'_{echem} > 1$ from eqn. (8). The overall solar energy conversion efficiency of water-splitting is constrained by the product of the available solar energy electronic conversion efficiency, η_{phot}, with the water electrolysis energy conversion efficiency.[5] For solar photo-thermal water electrolysis, a portion of the solar spectrum will be used to drive charge transfer, and an unused, separate portion of the insolation will be used to raise ambient water to a temperature T:

$$\eta_{solar} = \eta_{phot}r\eta_{echem} = \eta_{phot}\cdot 1.229/V_{H_2O}(T) \qquad (9)$$

Conditions of $\eta_{solar} > \eta_{phot}$ will be shown to place specific restrictions on the photosensitizer. When $V_{H_2O} < E_{tneut}$, heat must flow to compensate cooling which occurs at the electrolysis rate, that is, for an enthalpy balanced system any additional required heat must flow in a flux equivalent to $i_{heat} = i_{H_2O}$, and at an average power P_{heat}, such that:

$$E_{tneut} = V_{H_2O} + P_{heat}/i_{H_2O} \qquad (10)$$

A photoelectrolysis system can contain multiple photo harvesting units and electrolysis units, where the ratio of electrolysis to photovolatic units is defined as R. Efficient water-splitting occurs with the system configured to match the water electrolysis and photopower maximum power point, in which a photo-driven charge from a photon flux generates a current density (electrons per unit area) to provide the two stoichiometric electrons per split water molecule. For example, due to a low photo-potential, a photo-driven charge from three serially-arranged Si energy gap devices may be required to dissociate a single room temperature water molecule. Alternately, as in a multiple bandgap device such as AlGaAs/GaAs, the high potential of a single photodriven charge may be sufficient to dissocate two water molecules.

For this hybrid solar driven charge transfer, the power is described by the product of the insolation power, P_{sun}, with η_{phot}, which is then applied to electrolysis, $\eta_{phot}P_{sun} = P_{echem} = i_{H_2O}V_{H_2O}$. Rearranging for i_{H_2O}, and substitution into eqn. (10), yields for heat balanced solar electrolysis at conditions of T and p, initiating with 25 °C, 1 bar water:

$$E_{tneut} = 1.481\ V = V_{H_2O}(T,p)\ (1 + P_{heat}/\eta_{phot}P_{sun}) \qquad (11)$$

Fig. 3 presents the available insolation power, $P_{\lambda_{max}}$ (mW cm^{-2}) of the integrated solar spectrum up to a minimum electronic excitation frequency, ν_{min}(eV), determined by integrating the solar spectral irradiance, S (mWcm^{-2}nm^{-1}), as a function of a maximum insolation wavelength, λ_{max}(nm). This $P_{\lambda_{max}}$ is calculated for the conventional terrestrial

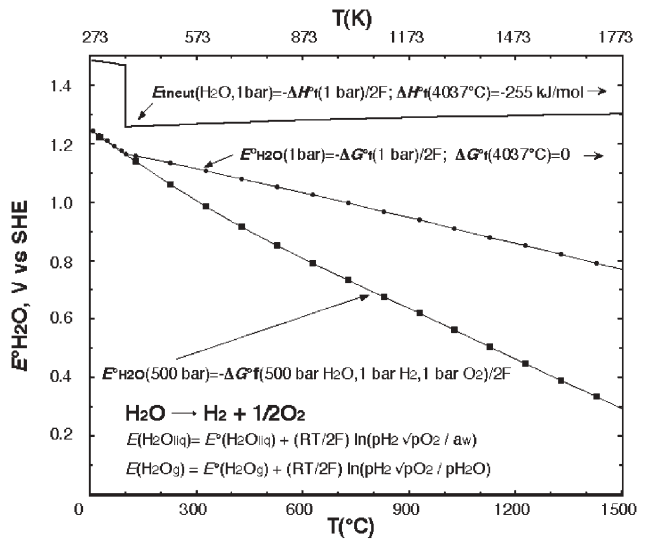

Fig. 2 Thermodynamic and electrochemical values for water dissociation to H_2 and O_2 as a function of temperature, as calculated in ref. 3. The $pH_2O = 1$ bar curves without squares are for liquid water through 100 °C and for steam at higher temperatures. The high pressure values curve ($pH_2O = 500$ bar; $pH_2 = pO_2 = 1$ bar) occurs at potential lower than that of 1 bar water. Note, the density of the high pressure fluid is similar to that of the liquid and may be generated in a confined space by heating or electrolyzing liquid water.

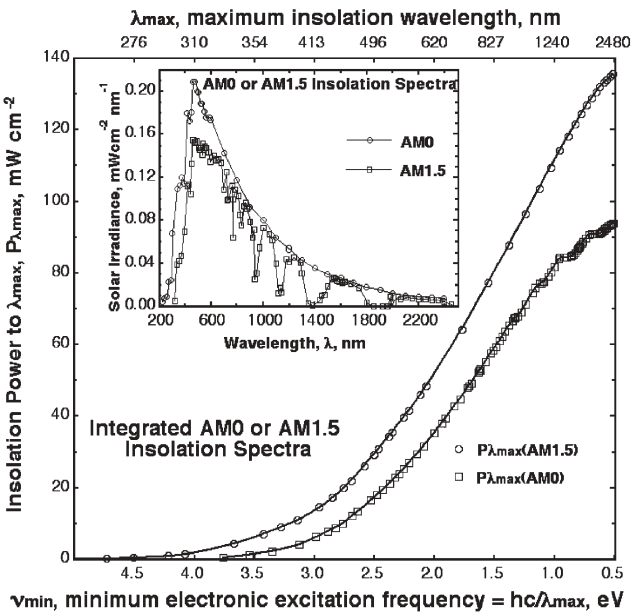

Fig. 3 Solar irradiance (mW cm^{-2} nm^{-1}) is in the figure inset, and total insolation power (mW cm^{-2}) is in the main figure of the solar spectrum.[3]

insolation spectrum either above the atmosphere, AM0, or through a 1.5 atmosphere pathway, AM1.5. Relative to the total power, P_{sun}, of either the AM0 or AM1.5 insolation, the fraction of this power available through the insolation edge is designated $P_{rel} = P_{\lambda_{max}}/P_{sun}$. In solar energy-balanced electrolysis, excess heat is available primarily as photons without sufficient energy for electronic excitation. The fraction these sub-bandgap photons in insolation is $\alpha_{heat} = 1 - P_{rel}$, and comprises an incident power of $\alpha_{heat}P_{sun}$.

Fig. 4 presents the variation of the minimum electronic excitation frequency, ν_{min} with α_{heat}, determined from P_{rel} using the values of $P_{\lambda_{max}}$ summarized in Fig. 3. A semiconductor sensitizer is constrained not to utilize incident energy below the bandgap. As seen in Fig. 4 by the intersection of the solid line with ν_{min}, over one third of insolation power occurs at $\nu_{min} < 1.43$ eV (867 nm), equivalent to the IR not absorbed by GaAs or wider bandgap materials. The calculations include both the AM0 and AM1.5 spectra. In the relevant visible and IR range from 0.5 to 3.1 eV (± 0.03 eV) for AM1.5 insolation spectra, $\nu_{min}(\alpha_{heat,})$, eV is well represented ($R^2 \geqslant 0.999$) by the polynomial fits:

$$\nu_{AM0} = 0.53008 + 3.1405\alpha_{heat} - 3.0687\alpha_{heat}^2 + 2.9103\alpha_{heat}^3 \quad (12)$$

When captured at a thermal efficiency of η_{heat}, the sub-bandgap insolation power is $\eta_{heat}\alpha_{heat}P_{sun}$. Other available system heating sources include absorbed super-bandgap photons which do not effectuate charge separation, P_{recomb}, and non-insolation sources, P_{amb}, such as heat available from the ambient environment heat sink, and P_{recov}, such as heat recovered from process cycling or subsequent H_2 fuel utilization. The power equivalent for losses, such as the low power consumed in delivering the heated water to electrolysis, P_{pump}, can also be incorporated. Together these comprise the power for heat balanced electrolysis, which with P_{heat} from eqn. (11) yields α_{heat}:

$$P_{heat} = \eta_{heat}\alpha_{heat}P_{sun} + \beta;\ \beta = P_{recomb} + P_{amb} + P_{recov} - P_{pump} \quad (13)$$

$$\alpha_{heat} = [\eta_{phot}/\eta_{heat}][\{1.481\ V/(1+\zeta)E^{\circ}_{H_2O} - 1\} - \beta/(\eta_{heat}P_{sun})] \quad (14)$$

For solar electrolysis at T,p, a minimum insolation energy, ν_{min}, leaves available for transmittance the requisite thermal energy. This constrains the minimum electronic excitation energy and the bandgap, $E_{g\text{-}min}$, which is determined from eqn. (12) using α_{heat} values estimated from eqn. (14):

$$E_{g\text{-}min} = \nu_{min}(P_{sun},\alpha_{heat});\ E_{g\text{-}min}(AM1.5) = \nu_{AM1.5}(\alpha_{heat})$$
$$\alpha_{heat}(T,p) \cong (\eta_{phot}/\eta_{heat})((1.481\ V/E^{\circ}_{H_2O}(T,p)) - 1) \quad (15)$$

A value of $\zeta = 0$ will overestimate, and $\beta = 0$ will underestimate, α_{heat} in eqn. (14) as presented in eqn. (15). Contemporary commercial alkaline water electrolysis cells exhibit overall $\zeta \cong 0.15$,[3] and large surface areas alkaline electrolysis cells sustain $\zeta < 0.05$.[5] Furthermore, ζ tends to diminish with increasing T, facilitating V_{H_2O} which approach $E^{\circ}_{H_2O}$ at elevated temperatures, and consistent with the rigorous upper limit for the solar electrolysis efficiency from eqn. (9):

$$\eta_{solar\text{-}max}(T,p) = 1.229\ \eta_{phot}/E^{\circ}_{H_2O}\ (T,p) \quad (16)$$

Fig. 5 determines the constraints on η_{solar} for various values of η_{phot}. These determinations of the solar water-splitting energy conversion are calculated from eqn. (16) using the $E^{\circ}_{H_2O}(T,p)$ data in Fig. 2, and for various solar water-splitting system's minimum allowed bandgap, $E_{g\text{-}min}(T,p)$ from eqn. (15) for a wide temperature range. The left side of Fig. 5 is for $p_{H_2O} = 1$ bar, and the right side calculated for $p_{H_2O} = 500$ bar. The rate of increase of $\eta_{solar\text{-}max}$ with temperature is significantly greater for higher pressure photoelectrolysis ($p_{H_2O} = 500$ bar). However as seen, at these higher pressures, higher efficiencies are offset by lower accessible temperatures (for a given bandgap). Larger ζ in V_{H_2O} will diminish η_{solar}, but will extend the usable small bandgap range. The upper end of experimental contemporary solar conversion efficiencies ranges from $100\eta_{phot} = 19.8\%$ for multicrystalline single junction photovoltaics, to 27.6% and 32.6% for single junction and multiple junction photovoltaics.[3] The efficiency of solar thermal conversion is higher, particularly for restricted spectral range absorption; and values of $\eta_{heat} = 0.5$, 0.7 or 1 are utilized for eqn. (15). While a small bandgap, $E_g < 1.23$ eV, is insufficient for water cleavage at 25 °C, its inclusion is of relevance in two cases, (i) high temperature decreases $V_{H_2O}(T)$ to below E_g and (ii) when it is part of a multiple bandgap contributing a portion of a larger overall photopotential. Note that $E_g > 3.0$ eV is inadequate for an efficient use of insolation.

Representative results from Fig. 5 for solar water-splitting to H_2 systems from AM1.5 insolation include a 50% solar

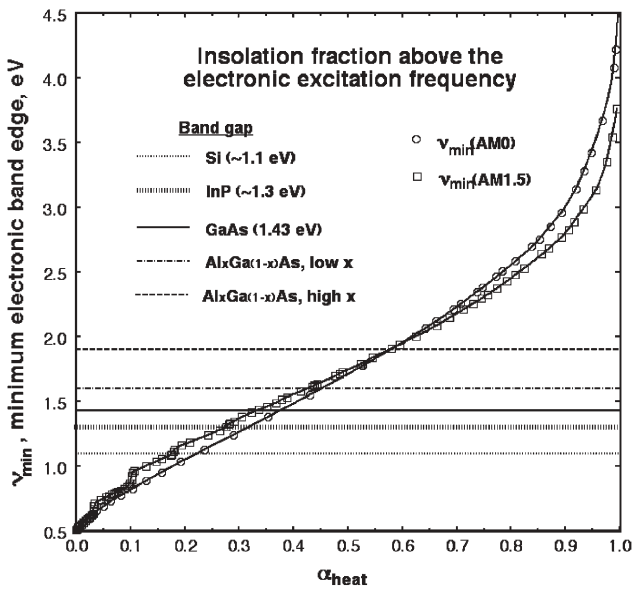

Fig. 4 $\alpha_{heat} = 1 - P_{rel}$, the fraction of solar energy available below ν_{min},[3] with $P_{rel} = P_{\lambda}/P_{sun}$. Available incident power below ν_{min} is $\alpha_{heat}P_{sun}$. Various semiconductor bandgaps are superimposed as vertical lines.

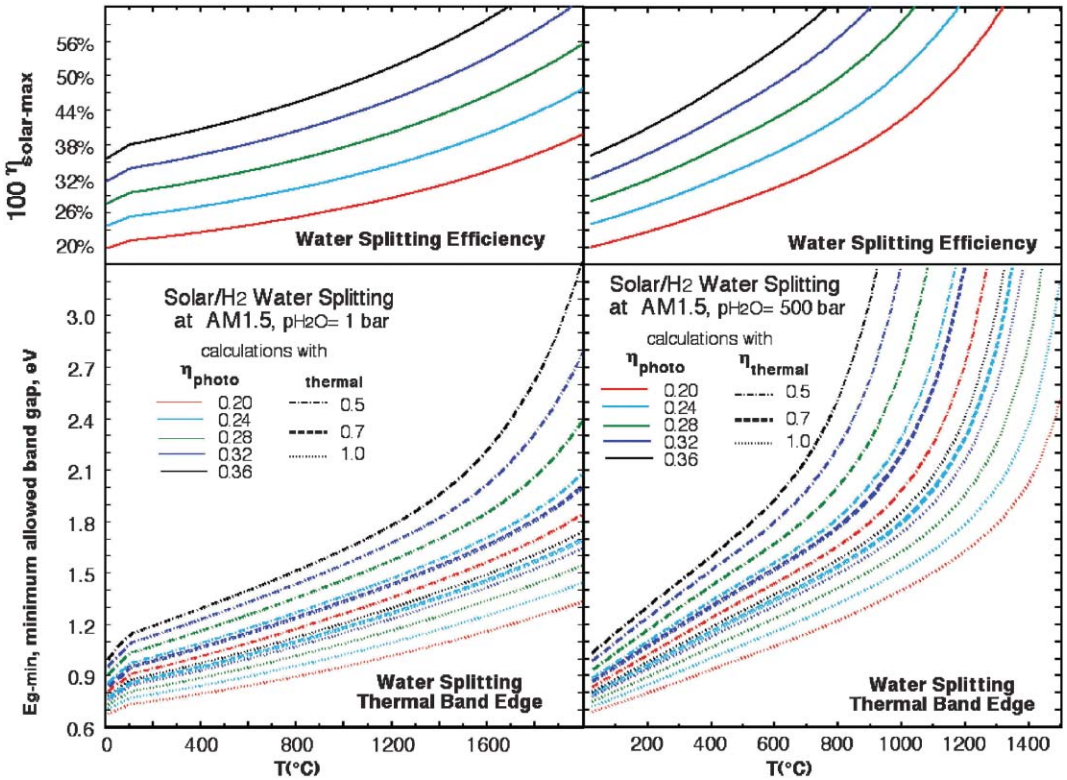

Fig. 5 Solar to H_2 conversion efficiency calculated at AM1.5 and at p_{H_2O} = 1 bar (left side), and at p_{H_2O} = 500 bar (right side).[3]

energy conversion for a photoelectrolysis system at 638 °C with p_{H_2O} = 500; p_{H_2} = 1 bar and η_{phot} = 0.32. However, this high H_2O partial pressure system requires separation of a low partial pressure of H_2. Efficient photoelectrolysis is also determined for high relative H_2, such as for systems of p_{H_2} = p_{H_2O} = 1 bar, η_{heat} = 0.7, and with a $E_{g\text{-}min}$ = E_g(GaAs) = 1.43 eV, in which efficiencies improve in Fig. 5 from 28% (at 25 °C) to 42% at 1360 °C, or from 32%(25 °C) to 46% at 1210 °C, or from 36%(25 °C) to 49% at 1060 °C. The case of the GaAs bandgap is of interest, as efficient multiple bandgap photovoltaics have also been demonstrated using GaAs as the semiconductor minimum bandgap component. ζ generated electrolysis heat is intrinsic to V_{H_2O}, and will diminish η_{solar}, but extend the small bandgap range, $E_{g\text{-}min}$. Consistent with the larger heat available up to α_{heat} = 0.6 in Fig. 4, moderately higher temperatures are accessible for fixed values of $E_{g\text{-}min}$ in Fig. 5.

Experiment into the efficient solar thermal hybrid/H_2 processes

Fletcher, repeating the fascinating suggestion of Brown that saturated aqueous NaOH will never boil, hypothesized that a useful medium for water electrolysis might be very high temperature NaOH saturated, aqueous solutions. These do not reach a temperature at which they boil at 1 atm due to the high salt solubility, binding solvent, and changing saturation vapor pressure, as reflected in their phase diagram.[44] We measured this domain, and also electrolysis in an even higher temperature domain above which NaOH melts (318 °C) creating a molten electrolyte with dissolved water, resulting in unexpected V_{H_2O}.

Fig. 6 summarizes the measured V_{H_2O} (T) in aqueous saturated and molten NaOH electrolytes. As seen in the inset, Pt exhibits low overpotentials to H_2 evolution, and is used as a convenient quasi-reference electrode in the measurements which follow. As also seen in the inset, Pt exhibits a known large overpotential to O_2 evolution as compared to a Ni electrode or to $E^\circ_{H_2O}$(25 °C) = 1.23 V. This overpotential loss

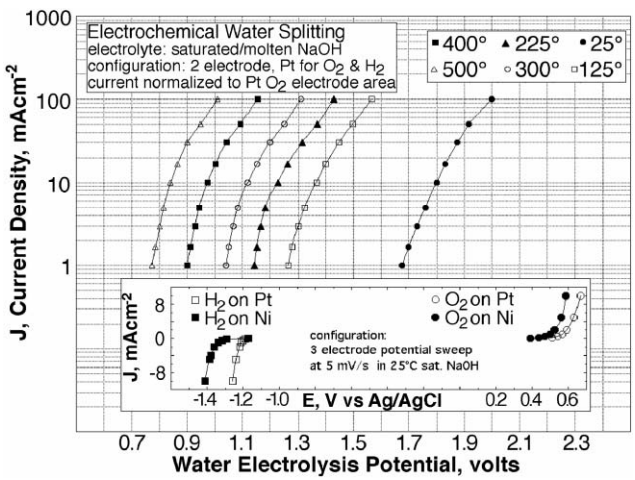

Fig. 6 V_{H_2O}, measured in aqueous saturated or molten NaOH, at 1 atm. The molten electrolyte is prepared from heated, solid NaOH with steam injection. The O_2 anode is 0.6 cm^2 Pt foil. IR and polarization losses are minimized by sandwiching 5 mm from each side of the anode, two interconnected Pt cathodes. Fig. inset: At 25°, 3 electrode values at 5 mVs^{-1} *versus* Ag/AgCl, with either 0.6 cm^2 Pt or Ni foil.[40]

diminishes at moderately elevated temperatures, and as seen in the main portion of the figure, at 125 °C there is a 0.4 V decrease in the O_2 activation potential at a Pt surface. Through 300 °C in Fig. 6, measured V_{H_2O} remains greater than the calculated thermodynamic rest potential. Unexpectedly, V_{H_2O} at 400 °C and 500 °C in molten NaOH occurs at values substantially smaller than that predicted. These measured values include voltage increases due to IR and hydrogen overpotentials and hence provide an upper bound to the unusually small electrochemical potential. Even at relatively large rates of water-splitting (30 mA cm^{-2}) at 1 atm, a measured V_{H_2O} in Fig. 6 is observed to be below that predicted by theory at temperatures above the 318 °C NaOH melting point in Fig. 2. Comparing the figures, the observed V_{H_2O} values at high temperature approach that calculated for a thermodynamic system of 500 bar, rather than at 1 bar, H_2O.

A source of the nominally less than thermodynamic water splitting potentials is described in Scheme 4. Shown on the left hand is the single compartment cell utilized here. Cathodically generated H_2 is in close proximity to the anode, while anodic O_2 is generated near the cathode. Their presence will facilitate the water-forming back reaction, and at the electrodes this recombination will diminish the potential. In addition to the observed low potentials, two observations support this recombination effect. The generated H_2 and O_2 is collected, but is consistent with a coulombic efficiency of ≈50% (varying with T, j and interelectrode separation). Consistent with the right hand side of Scheme 4, when conducted in separated anode/cathode compartments, this observed efficiency is 98%–100%. Here, however, all cell open circuit potentials increase to beyond the thermodynamic potential, and at j = 100 mA cm^{-2} yields measured V_{H_2O} values of 1.45 V, 1.60 V, 1.78 V at 500°, 400°, and 300°, which are approximately 450 mV higher than the equivalent values for the single configuration cell.

The recombination phenomenon offers advantages (low V_{H_2O}), but also disadvantages (H_2 losses), requiring study to balance these competing effects to optimize energy efficiency. In molten NaOH, temperature variation effects of $\Delta G^\circ_f(H_2O)$ and the recombination of the water splitting products can have a pronounced effect on solar driven electrolysis. As compared to 25 °C data in Fig. 6, only half the potential is required to split water at 500 °C, over a wide current density range.

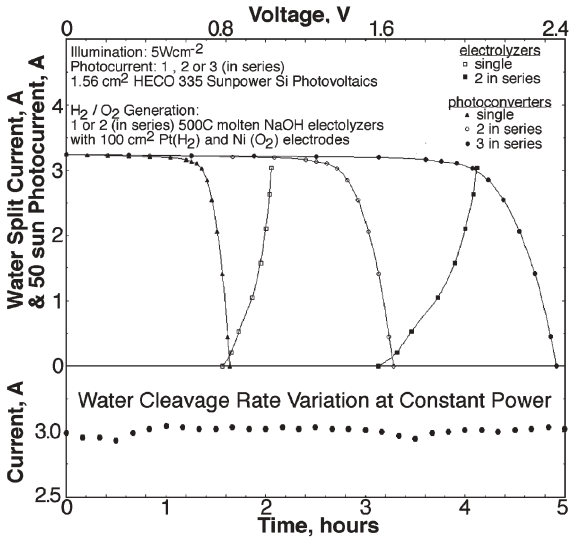

Fig. 7 Photovoltaic and electrolysis charge transfer for thermal electrochemical solar driven water-splitting. Photocurrent is shown for 1, 2 or three 1.561 cm^2 HECO 335 Si photovoltaics in series at 50 suns which drive 500 °C molten NaOH steam electrolysis using Pt gauze anode and cathodes. Inset: electrolysis current stability.[40]

The unused thermal photons which are not required in semiconductor photodriven charge generation, can contribute to heating water to facilitate electrolysis at an elevated temperature. The characteristics of one, two, or three series interconnected solar visible efficient photosensitizers, in accord with the manufacturer's calibrated standards, are presented in Fig. 7. These silicon photovoltaics are designed for efficient photoconversion under concentrated insolation (η_{solar} = 26.3% at 50 suns). Superimposed on the photovoltaic response curves in the figure are the water electrolysis current densities for one, or two series interconnected, 500 °C molten NaOH single compartment cell configuration electrolyzers.

Constant illumination, generates for the three series cells, a constant photopotential for stability measurements at sufficient power to drive two series molten NaOH electrolyzers. At this constant power, and as presented in the lower portion of Fig. 7, the rate of water-splitting appears fully stable over an extended period. In addition, as measured and summarized in

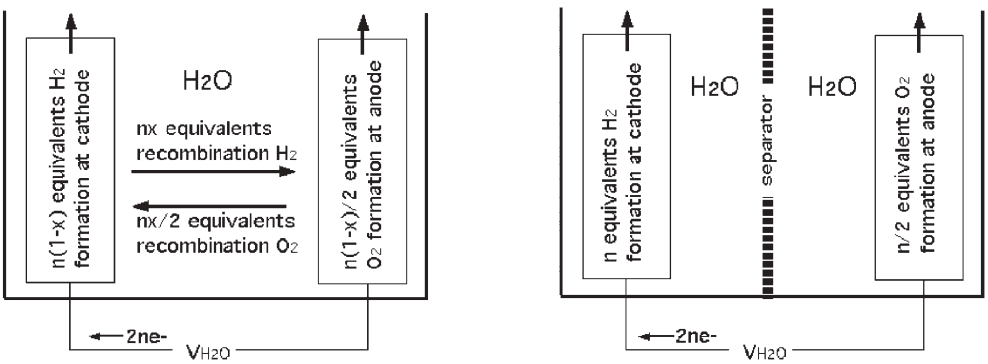

Scheme 4 Inter-electrode recombination can diminish V_{H_2O} and occurs in open (left), but not in isolated (right), configurations; such as with or without a Zr_2O mix fiber separator between the Pt electrodes.[40]

the upper portion of the figure, for the overlapping region between the solid triangle and open square curves, a single Si photovoltaic can drive 500 °C water-splitting, albeit at an energy beyond the maximum power point voltage, and therefore at diminished efficiency. This appears to be the first case in which an external, single, small bandgap photosentizer can cleave water, and is accomplished by tuning the water-splitting electrochemical potential to decrease below the Si open circuit photovoltage. $V_{H_2O\text{-tuned}}$ is accomplished by two phenomena: (i) the thermodynamic decrease of E_{H_2O} with increasing temperature, and (ii) a partial recombination of the water-splitting products. $V_{H_2O\text{-tuned}}$ can drive system efficiency advances, *e.g.* AlGaAs/GaAs, transmits more insolation, $E_{IR} < 1.4$ eV, than Si to heat water, and with η_{photo} over 30%, prior to system engineering losses, calculates to over 50% η_{solar} to H_2.

Fundamental details of splitting of the thermal and visible insolation, with the former to heat water for electrolysis, and the latter to drive electrical charge formation, have been presented. In addition, experimental components, of the representation described in Scheme 3, of efficient solar driven generation of H_2 fuel at 40–50% solar energy conversion efficiencies appear to be technologically available. Without inclusion of high temperature effects, we had already experimentally achieved $\eta_{solar} > 0.18$, using an $\eta_{phot} = 0.20$ AlGaAs/Si system.[5] Our use of more efficient, ($\eta_{phot} = 26.3\%$ at 50 sun, and inclusion of heat effects and the elevated temperature decrease of the water electrolysis potential, substantially enhances, η_{solar}.[40] Existing, higher $\eta_{phot} = 0.28$ to 0.33 systems should achieve proportionally higher results.

Photoelectrochemical cells tend to be unstable, which is likely to be exacerbated at elevated temperatures. Hence, the hybrid solar/thermal hydrogen process will be particularly conducive to photovoltaic, rather than photoelectrochemical, driven electrolysis. The photovoltaic component is used for photodriven charge into the electrolysis component, but does not contact the heated electrolyte. In this case the high efficiencies appear accessible, stable photovoltaics are commonly driven with concentrated insolation and specific to the system model here, heat will be purposely filtered from the insolation prior to incidence on the photovoltaic component.

Dielectric filters used in laser optics split insolation without absorption losses. For example, in a system based on a parabolic concentrator, a casegrain configuration may be used, with a mirror made from fused silica glass with a dielectric coating acting as band pass filter. The system will form two focal spots with different spectral configuration, one at the focus of the parabola and the other at the focus of the casegrain.[45] The thermodynamic limit of concentration is 46 000 suns, the brightness of the surface of the sun. In a medium with refractive index greater than one, the upper limit is increased by 2 times the refractive index, although this value is reduced by reflective losses and surface errors of the reflective surfaces, the tracking errors of the mirrors and dilution of the mirror field. Specifically designed optical absorbers, such as parabolic concentrators or solar towers, can efficiently generate a solar flux with concentrations of $\sim$2000 suns, generating temperatures in excess of 1000 °C.[46]

Commercial alkaline electrolysis occurs at temperatures up to 150 °C and pressures to 30 bar, and super-critical electrolysis to 350 °C and 250 bar.[47] Although less developed than their fuel cell counterparts which have 100 kW systems in operation and developed from the same oxides,[48] zirconia and related solid oxide based electrolytes for high temperature steam electrolysis can operate efficiently at 1000 °C,[49] and approach the operational parameters necessary for efficient solar driven water-splitting. Efficient multiple bandgap solar cells absorb light up to the bandgap of the smallest bandgap component. Thermal radiation is assumed to be split off (removed and utilized for water heating) prior to incidence on the semiconductor and hence will not substantially effect the bandgap. Highly efficient photovoltaics have been demonstrated at a solar flux with a concentration of several hundred suns. AlGaAs/GaAs has yielded at η_{phot} efficiency of 27.6%, and a GaInP/GaAs cell 30.3% at 180 suns concentration, while GaAs/Si has reached 29.6% at 350 suns, InP/GaInAs 31.8%, and GaAs/GaSb 32.6% with concentrated insolation, and new approaches using semiconductor nanoparticles for photovoltaic cells have been reported.[3,50]

Conclusions

Solar energy driven water-splitting combines several attractive features for energy utilization. The energy source (sun) and reactive media (water) for solar water-splitting are readily available and are renewable, and the resultant fuel (generated H_2) and its discharge product (water) are each environmentally benign. An overview of solar thermal processes for the generation of hydrogen is presented, and compared to alternate solar hydrogen processes. In particular, a hybrid solar thermal/electrochemical process combines efficient photovoltaics and concentrated excess sub-bandgap heat into highly efficient elevated temperature solar electrolysis of water and generation of H_2 fuel. Efficiency is further enhanced by excess super-bandgap and non-solar sources of heat, but diminished by losses in polarization and photo-electrolysis power matching. Solar concentration can provide the high temperature and diminish the requisite surface area of efficient electrical energy conversion components, and high temperature electrolysis components are available, suggesting that combination into highly efficient solar generation of H_2 will be attainable.

Notes and references

1 A. Kogan, *Int. J. Hydrogen Energy*, 1998, **23**, 89.
2 A. Steinfeld, *Sol. Energy*, 2005, **78**, 603.
3 S. Licht, *Int. J. Hydrogen Energy*, 2005, **30**, 459.
4 J. E. Funk, *Int. J. Hydrogen Energy*, 2001, **26**, 185.
5 S. Licht, B. Wang, S. Mukerji, T. Soga, M. Umeno and H. Tributsh, *Int. J. Hydrogen Energy*, 2001, **26**, 653.
6 T. Ohmori, H. Go, N. Yamaguchi, A. Nakayama, H. Mametisuka and E. Suzuki, *Int. J. Hydrogen Energy*, 2001, **26**, 661.
7 T. Tani, N. Sekiguchi, M. Sakai and D. Otha, *Sol. Energy*, 2000, **68**, 143.
8 M. P. Rzayeva, O. M. Salamov and M. K. Kerimov, *Int. J. Hydrogen Energy*, 2001, **26**, 195.
9 S. Licht, *J. Phys., Chem., B*, 2001, **105**, 6281.
10 S. Licht, H. Tributsch, S. Ghosh and S. Fiechter, *Sol. Energy Mater. Sol. Cells*, 2002, **70**, 4, 471.
11 S. Licht, *Nature*, 1987, **330**, 148.

12 S. Licht, G. Hodes, R. Tenne and J. Manassen, *Nature*, 1987, **326**, 863.
13 S. Licht, B. Wang, T. Soga and M. Umeno, *J. Appl. Phys. Lett.*, 1999, **74**, 4055.
14 B. Wang, S. Licht, T. Soga and M. Umeno, *Sol. Energy Mater. Sol. Cells*, 2000, **64**, 311.
15 S. Licht and D. Peramunage, *Nature*, 1990, **345**, 330.
16 S. Licht and D. Peramunage, *Nature*, 1991, **354**, 440.
17 S. Licht, *Sol. Energy Mater. Sol. Cells*, 1995, **38**, 305.
18 S. Licht and D. Peramunage, *J. Phys. Chem*, 1996, **100**, 9082.
19 Semiconductor Electrodes and Photoelectrochemistry, ed. S. Licht, Wiley-VCH, Weinheim, Germany, 2002.
20 A. Fujishima and K. Honda, *Nature*, 1972, **37**, 238.
21 A. Heller, E. Asharon-Shalom, W. A. Bonner and B. Miller, *J. Am. Chem. Soc.*, 1982, **104**, 6942.
22 O. Khaselev and J. A. Turner, *Science*, 1998, **280**, 425427.
23 S. Licht, B. Wang, S. Mukerji, T. Soga, M. Umeno and H. Tributsch, *J. Phys., Chem., B*, 2000, **104**, 8920.
24 H. Ohya, M. Yatabe, M. Aihara, Y. Negishi and T. Takeuchi, *Int. J. Hydrogen Energy*, 2002, **27**, 369.
25 E. A. Fletcher and R. L. Moen, *Science*, 1977, **197**, 105.
26 J. Lede, J. Villermaux, R. Ouzane, M. A. Hossain and R. Ouahes, *Int. J. Hydrogen Energy*, 1987, **12**, 3.
27 A. Yogev, A. Kribus, M. Epstein and A. Kogan, *Int. J. Hydrogen Energy*, 1998, **26**, 239.
28 A. Kogan, *Int. J. Hydrogen Energy*, 2000, **25**, 1043.
29 H. Naito and H. Arashi, *Solid State Ionics*, 1995, **79**, 366.
30 R. P. Omorjan, R. N. Paunovic, M. N. Tekic and M. G. Antov, *Int. J. Hydrogen Energy*, 2001, **26**, 203.
31 S. Z. Baykara, *Int. J. Hydrogen Energy*, 2004, **29**, 1459.
32 N. Serpone, D. Lawless and R. Terzian, *Sol. Energy*, 1992, **49**, 221.
33 R. Palumbo, J. Lede, O. Boutin, E. Elorza Ricart, A. Steinfeld, S. Moeller, A. Weidenkaff, E. A. Fletcher and J. Bielicki, *Chem. Eng. Sci.*, 1998, **53**, 2503.
34 C. Perkins and A. W. Weimer, *Int. J. Hydrogen Energy*, 2004, **29**, 1587.
35 H. Kaneko, N. Gokon, N. Hasewaga and Y. Tamaura, *Energy*, 2005, **30**, 2171.
36 A. J. DeBethune, T. S. Licht and N. S. Swendemna, *J. Electrochem. Soc.*, 1959, **106**, 618.
37 J. O'M. Bockris, *Energy Options*, Halsted Press, NY, p. 1980.
38 S. Licht, *Electrochem. Commun.*, 2002, **4**, 790.
39 S. Licht, *J. Phys. Chem. B*, 2002, **107**, 4253.
40 S. Licht, L. Halperin, M. Kalina, M. Zidman and N. Halperin, *Chem. Commun.*, 2003, 3006.
41 S. Licht, *Anal. Chem.*, 1987, **57**, 514.
42 T. S. Light, T. S. Licht, A. C. Bevilacqua and R. Morash Kenneth, *Electrochem. Solid State Lett.*, 2005, **8**, E16.
43 S. Licht, *Electroanal. Chem.*, ed. A. Bard, I. Rubinstein, Marcel Dekker, NY, 1998, vol. 20, p. 87.
44 E. Fletcher, *J. Sol. Energy Eng.*, 2001, **123**, 143.
45 A. Yogev, *Weizmann Sun Symp. Proc.*, Rehovot, Israel, 1996.
46 E. Segal and M. Epstein, *Sol. Energy*, 2001, **69**, 229.
47 B. Misch, A. Firus and G. Brunner, *J. Supercrit. Fluids*, 2000, **17**, 227.
48 O. Yamamoto, *Electrochim. Acta*, 2000, **45**, 2423.
49 K. Eguchi, T. Hatagishi and H. Arai, *Solid State Ionics*, 1996, **86–8**, 1245.
50 M. A. Green, *Sol. Energy*, 2004, **76**, 3.

